23. COSMIC MICROWAVE BACKGROUND

Revised August 2005 by D. Scott (University of British Columbia) and G.F. Smoot (UCB/LBNL).

23.1. Introduction

The energy content in radiation from beyond our Galaxy is dominated by the Cosmic Microwave Background (CMB), discovered in 1965 [1]. The spectrum of the CMB is well described by a blackbody function with $T = 2.725\,\mathrm{K}$. This spectral form is one of the main pillars of the hot Big Bang model for the early Universe. The lack of any observed deviations from a blackbody spectrum constrains physical processes over cosmic history at redshifts $z \lesssim 10^7$ (see previous versions of this mini-review). However, at the moment, all viable cosmological models predict a very nearly Planckian spectrum, and so are not stringently limited.

Another observable quantity inherent in the CMB is the variation in temperature (or intensity) from one part of the microwave sky to another [2]. Since the first detection of these anisotropies by the *COBE* satellite [3], there has been intense activity to map the sky at increasing levels of sensitivity and angular resolution. A series of ground- and balloon-based measurements was joined in 2003 by the first results from NASA's Wilkinson Microwave Anisotropy Probe (*WMAP*) [4]. These observations have led to a stunning confirmation of the 'Standard Model of Cosmology.' In combination with other astrophysical data, the CMB anisotropy measurements place quite precise constraints on a number of cosmological parameters, and have launched us into an era of precision cosmology.

23.2. Description of CMB Anisotropies

Observations show that the CMB contains anisotropies at the 10^{-5} level, over a wide range of angular scales. These anisotropies are usually expressed by using a spherical harmonic expansion of the CMB sky:

$$T(\theta,\phi) = \sum_{\ell m} a_{\ell m} Y_{\ell m}(\theta,\phi).$$

The vast majority of the cosmological information is contained in the temperature 2 point function, *i.e.*, the variance as a function of separation θ. Equivalently, the power per unit $\ln \ell$ is $\ell \sum_m |a_{\ell m}|^2 / 4\pi$.

23.2.1. *The Monopole*:

The CMB has a mean temperature of $T_\gamma = 2.725 \pm 0.001\,\mathrm{K}$ (1σ) [5], which can be considered as the monopole component of CMB maps, a_{00}. Since all mapping experiments involve difference measurements, they are insensitive to this average level. Monopole measurements can only be made with absolute temperature devices, such as the FIRAS instrument on the *COBE* satellite [5]. Such measurements of the spectrum are consistent with a blackbody distribution over more than three decades in frequency. A blackbody of the measured temperature corresponds to $n_\gamma = (2\zeta(3)/\pi^2)\,T_\gamma^3 \simeq 411\,\mathrm{cm}^{-3}$ and $\rho_\gamma = (\pi^2/15)\,T_\gamma^4 \simeq 4.64 \times 10^{-34}\,\mathrm{g\,cm}^{-3} \simeq 0.260\,\mathrm{eV\,cm}^{-3}$.

23.2.2. *The Dipole*:

The largest anisotropy is in the $\ell = 1$ (dipole) first spherical harmonic, with amplitude $3.346 \pm 0.017\,\mathrm{mK}$ [4]. The dipole is interpreted to be the result of the Doppler shift caused by the solar system motion relative to the nearly isotropic blackbody field, as confirmed by measurements of the radial velocities of local galaxies [6]. The motion of an observer with velocity $\beta = v/c$ relative to an isotropic Planckian radiation field of temperature T_0 produces a Doppler-shifted temperature pattern

$$\begin{aligned} T(\theta) &= T_0(1-\beta^2)^{1/2}/(1-\beta\cos\theta) \\ &\approx T_0\left(1+\beta\cos\theta+(\beta^2/2)\cos 2\theta+O(\beta^3)\right). \end{aligned}$$

At every point in the sky one observes a blackbody spectrum, with temperature $T(\theta)$. The spectrum of the dipole is the differential of a blackbody spectrum, as confirmed by Ref. 7.

The implied velocity [8,4] for the solar system barycenter is $v = 368 \pm 2\,\mathrm{km\,s^{-1}}$, assuming a value $T_0 = T_\gamma$, towards $(\ell, b) = (263.85^\circ \pm 0.10^\circ, 48.25^\circ \pm 0.04^\circ)$. Such a solar system velocity implies a velocity for the Galaxy and the Local Group of galaxies relative to the CMB. The derived value is $v_{\mathrm{LG}} = 627 \pm 22\,\mathrm{km\,s^{-1}}$ towards $(\ell, b) = (276^\circ \pm 3^\circ, 30^\circ \pm 3^\circ)$, where most of the error comes from uncertainty in the velocity of the solar system relative to the Local Group.

The dipole is a frame dependent quantity, and one can thus determine the 'absolute rest frame' of the Universe as that in which the CMB dipole would be zero. Our velocity relative to the Local Group, as well as the velocity of the Earth around the Sun, and any velocity of the receiver relative to the Earth, is normally removed for the purposes of CMB anisotropy study.

23.2.3. *Higher-Order Multipoles*:

Excess variance in CMB maps at higher multipoles ($\ell \geq 2$) is interpreted as being the result of perturbations in the density of the early Universe, manifesting themselves at the epoch of the last scattering of the CMB photons. In the hot Big Bang picture, this happens at a redshift $z \simeq 1100$, with little dependence on the details of the model. The process by which the hydrogen and helium nuclei can hold onto their electrons is usually referred to as recombination [9]. Before this epoch, the CMB photons are tightly coupled to the baryons, while afterwards they can freely stream towards us.

Theoretical models generally predict that the $a_{\ell m}$ modes are Gaussian random fields. Tests show that this is an extremely good simplifying approximation [10], with only some relatively weak indications of non-Gaussianity or statistical anisotropy at large scales. Although non-Gaussianity of various forms is possible in early Universe models [11], the signatures found in existing *WMAP* data are generally considered to be subtle foreground or instrumental artefacts [12,13].

With the assumption of Gaussian statistics, and if there is no preferred axis, then it is the variance of the temperature field which carries the cosmological information, rather than the values of the individual $a_{\ell m}$s; in other words the power spectrum in ℓ fully characterizes the anisotropies. The power at each ℓ is $(2\ell+1)C_\ell/(4\pi)$, where

$C_\ell \equiv \langle |a_{\ell m}|^2 \rangle$, and a statistically isotropic sky means that all ms are equivalent. We use our estimators of the C_ℓs to constrain their expectation values, which are the quantities predicted by a theoretical model. For an idealized full-sky observation, the variance of each measured C_ℓ (*i.e.*, the variance of the variance) is $[2/(2\ell+1)]C_\ell^2$. This sampling uncertainty (known as 'cosmic variance') comes about because each C_ℓ is χ^2 distributed with $(2\ell+1)$ degrees of freedom for our observable volume of the Universe. For fractional sky coverage, $f_{\rm sky}$, this variance is increased by $1/f_{\rm sky}$ and the modes become partially correlated.

It is important to understand that theories predict the expectation value of the power spectrum, whereas our sky is a single realization. Hence the cosmic variance is an unavoidable source of uncertainty when constraining models; it dominates the scatter at lower ℓs, while the effects of instrumental noise and resolution dominate at higher ℓs [14].

23.2.4. *Angular Resolution and Binning*:

There is no one-to-one conversion between multipole ℓ and the angle subtended by a particular wavevector projected onto the sky. However, a single spherical harmonic $Y_{\ell m}$ corresponds to angular variations of $\theta \sim \pi/\ell$. CMB maps contain anisotropy information from the size of the map (or in practice some fraction of that size) down to the beam-size of the instrument, σ. One can think of the effect of a Gaussian beam as rolling off the power spectrum with the function $\mathrm{e}^{-\ell(\ell+1)\sigma^2}$.

For less than full sky coverage, the ℓ modes become correlated. Hence, experimental results are usually quoted as a series of 'band powers', defined as estimators of $\ell(\ell+1)C_\ell/2\pi$ over different ranges of ℓ. Because of the strong foreground signals in the Galactic Plane, even 'all-sky' surveys, such as *COBE* and *WMAP* involve a cut sky. The amount of binning required to obtain uncorrelated estimates of power also depends on the map size.

23.3. Cosmological Parameters

The current 'Standard Model' of cosmology contains around 10 free parameters (see The Cosmological Parameters—Sec. 21 of this *Review*). The basic framework is the Friedmann-Robertson-Walker metric (*i.e.*, a universe that is approximately homogeneous and isotropic on large scales), with density perturbations laid down at early times and evolving into today's structures (see Big-Bang cosmology—Sec. 19 of this *Review*). These perturbations can be either 'adiabatic' (meaning that there is no change to the entropy per particle for each species, *i.e.*, $\delta\rho/\rho$ for matter is $(3/4)\delta\rho/\rho$ for radiation) or 'isocurvature' (meaning that, for example, matter perturbations compensate radiation perturbations so that the total energy density remains unperturbed, *i.e.*, $\delta\rho$ for matter is $-\delta\rho$ for radiation). These different modes give rise to distinct phases during growth, with those of the adiabatic scenario being strongly preferred by the data. Models that generate mainly isocurvature type perturbations (such as most topological defect scenarios) are no longer considered to be viable.

Within the adiabatic family of models, there is, in principle, a free function describing how the comoving curvature perturbations, $\mathcal{R}$, vary with scale. In inflationary models [15], the Taylor series expansion of $\ln \mathcal{R}(\ln k)$ has terms of steadily decreasing size. For the simplest models, there are thus 2 parameters describing the initial conditions for

density perturbations: the amplitude and slope of the power spectrum, $\left\langle |\mathcal{R}|^2 \right\rangle \propto k^n$. This can be explicitly defined, for example, through:

$$\Delta^2_{\mathcal{R}} \equiv (k^3/2\pi^2) \left\langle |\mathcal{R}|^2 \right\rangle ,$$

and using $A^2 \equiv \Delta^2_{\mathcal{R}}(k_0)$ with $k_0 = 0.05\,\mathrm{Mpc}^{-1}$, say. There are many other equally valid definitions of the amplitude parameter (see also Sec. 19 and Sec. 21 of this *Review*), and we caution that the relationships between some of them can be cosmology dependent. In 'slow roll' inflationary models this normalization is proportional to the combination $V^3/(V')^2$, for the inflationary potential $V(\phi)$. The slope n also involves V'', and so the combination of A and n can, in principle, constrain potentials.

Inflation generates tensor (gravity wave) modes as well as scalar (density perturbation) modes. This fact introduces another parameter measuring the amplitude of a possible tensor component, or equivalently the ratio of the tensor to scalar contributions. The tensor amplitude $A_{\mathrm{T}} \propto V$, and thus one expects a larger gravity wave contribution in models where inflation happens at higher energies. The tensor power spectrum also has a slope, often denoted n_{T}, but since this seems likely to be extremely hard to measure, it is sufficient for now to focus only on the amplitude of the gravity wave component. It is most common to define the tensor contribution through r, the ratio of tensor to scalar perturbation spectra at large scales (say $k = 0.002\,\mathrm{Mpc}^{-1}$); however, there are other definitions in terms of the ratio of contributions to C_2, for example. Different inflationary potentials will lead to different predictions, e.g. for $\lambda\phi^4$ inflation with 50 e-folds, $r = 0.32$, while other models can have arbitrarily small values of r. In any case, whatever the specific definition, and whether they come from inflation or something else, the 'initial conditions' give rise to a minimum of 3 parameters: A, n, and r.

The background cosmology requires an expansion parameter (the Hubble Constant, H_0, often represented through $H_0 = 100\,h\,\mathrm{km\,s^{-1}Mpc^{-1}}$) and several parameters to describe the matter and energy content of the Universe. These are usually given in terms of the critical density, *i.e.*, for species 'x', $\Omega_{\mathrm{x}} = \rho_{\mathrm{x}}/\rho_{\mathrm{crit}}$, where $\rho_{\mathrm{crit}} = 3H_0^2/8\pi G$. Since physical densities $\rho_{\mathrm{x}} \propto \Omega_{\mathrm{x}} h^2 \equiv \omega_{\mathrm{x}}$ are what govern the physics of the CMB anisotropies, it is these ωs that are best constrained by CMB data. In particular CMB observations constrain $\Omega_{\mathrm{B}} h^2$ for baryons and $\Omega_{\mathrm{M}} h^2$ for baryons plus Cold Dark Matter.

The contribution of a cosmological constant Λ (or other form of Dark Energy) is usually included through a parameter which quantifies the curvature, $\Omega_{\mathrm{K}} \equiv 1 - \Omega_{\mathrm{tot}}$, where $\Omega_{\mathrm{tot}} = \Omega_{\mathrm{M}} + \Omega_{\Lambda}$. The radiation content, while in principle a free parameter, is precisely enough determined by the measurement of T_γ, and makes a negligible contribution to Ω_{tot} today.

The main effect of astrophysical processes on the C_ℓs comes through reionization. The Universe became reionized at some redshift z_{i}, long after recombination, affecting the CMB through the integrated Thomson scattering optical depth:

$$\tau = \int_0^{z_{\mathrm{i}}} \sigma_{\mathrm{T}} n_{\mathrm{e}}(z) \frac{dt}{dz} dz,$$

where σ_{T} is the Thomson cross-section, $n_{\mathrm{e}}(z)$ is the number density of free electrons (which depends on astrophysics) and dt/dz is fixed by the background cosmology. In

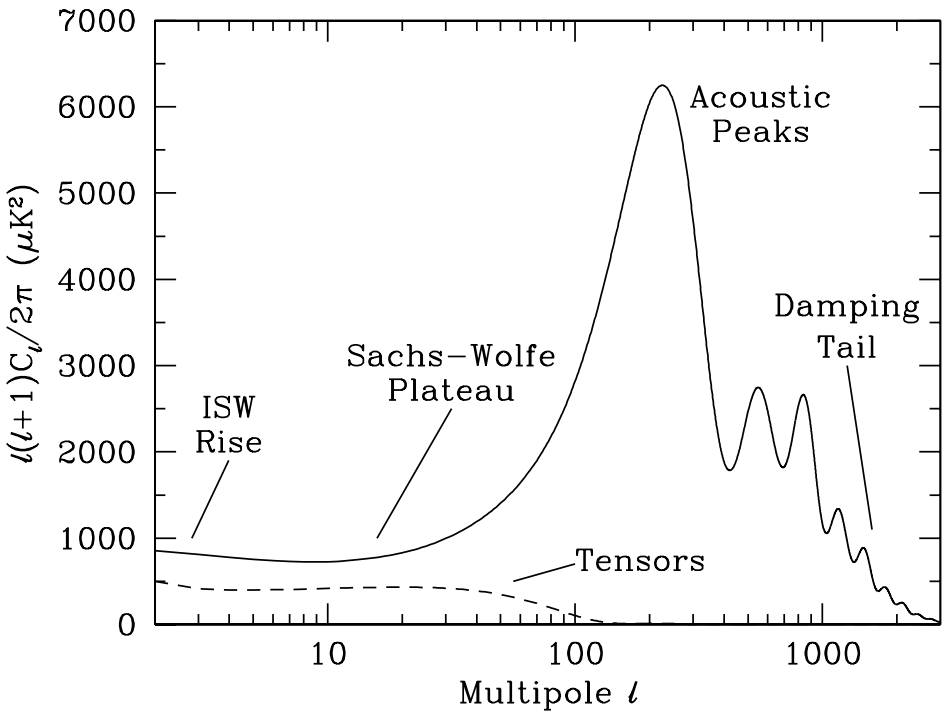

Figure 23.1: The theoretical CMB anisotropy power spectrum, using a standard ΛCDM model from CMBFAST. The x-axis is logarithmic here. The regions, each covering roughly a decade in ℓ, are labeled as in the text: the ISW Rise; Sachs-Wolfe Plateau; Acoustic Peaks; and Damping Tail. Also shown is the shape of the tensor (gravity wave) contribution, with an arbitrary normalization.

principle, τ can be determined from the small scale matter power spectrum together with the physics of structure formation and feedback processes. However, this is a sufficiently complicated calculation that τ needs to be considered as a free parameter.

Thus we have 8 basic cosmological parameters: A, n, r, h, $\Omega_{\rm B}h^2$, $\Omega_{\rm M}h^2$, $\Omega_{\rm tot}$, and τ. One can add additional parameters to this list, particularly when using the CMB in combination with other data sets. The next most relevant ones might be: $\Omega_\nu h^2$, the massive neutrino contribution; w ($\equiv p/\rho$), the equation of state parameter for the Dark Energy; and $dn/d\ln k$, measuring deviations from a constant spectral index. To these 11 one could of course add further parameters describing additional physics, such as details of the reionization process, features in the initial power spectrum, a sub-dominant contribution of isocurvature modes, *etc.*

As well as these underlying parameters, there are other quantities that can be obtained from them. Such derived parameters include the actual Ωs of the various components (*e.g.*, $\Omega_{\rm M}$), the variance of density perturbations at particular scales (*e.g.*, σ_8), the age of the Universe today (t_0), the age of the Universe at recombination, reionization, *etc.*

23.4. Physics of Anisotropies

The cosmological parameters affect the anisotropies through the well understood physics of the evolution of linear perturbations within a background FRW cosmology. There are very effective, fast, and publicly-available software codes for computing the CMB anisotropy, polarization, and matter power spectra, *e.g.*, `CMBFAST` [16] and `CAMB` [17]. `CMBFAST` is the most extensively used code; it has been tested over a wide range of cosmological parameters and is considered to be accurate to better than the 1% level [18].

A description of the physics underlying the C_ℓs can be separated into 3 main regions, as shown in Fig. 23.1.

23.4.1. *The Sachs-Wolfe plateau:* $\ell \lesssim 100$:

The horizon scale (or more precisely, the angle subtended by the Hubble radius) at last scattering corresponds to $\ell \simeq 100$. Anisotropies at larger scales have not evolved significantly, and hence directly reflect the 'initial conditions.' The combination of gravitational redshift and intrinsic temperature fluctuations leads to $\delta T/T \simeq (1/3)\delta\phi/c^2$, where $\delta\phi$ is the perturbation to the gravitational potential. This is usually referred to as the 'Sachs-Wolfe' effect [19].

Assuming that a nearly scale-invariant spectrum of density perturbations was laid down at early times (*i.e.*, $n \simeq 1$, meaning equal power per decade in k), then $\ell(\ell+1)C_\ell \simeq$ constant at low ℓs. This effect is hard to see unless the multipole axis is plotted logarithmically (as in Fig. 23.1, but not Fig. 23.2).

Time variation of the potentials (*i.e.*, time-dependent metric perturbations) leads to an upturn in the C_ℓs in the lowest several multipoles; any deviation from a total equation of state $w = 0$ has such an effect. So the dominance of the Dark Energy at low redshift makes the lowest ℓs rise above the plateau. This is sometimes called the 'integrated Sachs-Wolfe effect' (or ISW Rise), since it comes from the line integral of $\dot{\phi}$; it has been confirmed through correlations between the large-angle anisotropies and large-scale structure [20]. Specific models can also give additional contributions at low ℓ (*e.g.*, perturbations in the Dark Energy component itself [21]), but typically these are buried in the cosmic variance.

In principle, the mechanism that produces primordial perturbations could generate scalar, vector, and tensor modes. However, the vector (vorticity) modes decay with the expansion of the Universe. Tensors also decay when they enter the horizon, and so they contribute only to angular scales above about 1° (see Fig. 23.1). Hence some fraction of the low ℓ signal could be due to a gravity wave contribution, although small amounts of tensors are essentially impossible to discriminate from other effects that might raise the level of the plateau. However, the tensors *can* be distinguished using polarization information (see Sec. 23.6).

23.4.2. ***The acoustic peaks:*** $\mathbf{100 \lesssim \ell \lesssim 1000}$:

On sub-degree scales, the rich structure in the anisotropy spectrum is the consequence of gravity-driven acoustic oscillations occurring before the atoms in the Universe became neutral. Perturbations inside the horizon at last scattering have been able to evolve causally and produce anisotropy at the last scattering epoch, which reflects that evolution. The frozen-in phases of these sound waves imprint a dependence on the cosmological parameters, which gives CMB anisotropies their great constraining power.

The underlying physics can be understood as follows. Before the Universe became neutral the proton-electron plasma was tightly coupled to the photons, and these components behaved as a single 'photon-baryon fluid'. Perturbations in the gravitational potential, dominated by the dark matter component, were steadily evolving. They drove oscillations in the photon-baryon fluid, with photon pressure providing most of the restoring force and baryons giving some additional inertia. The perturbations were quite small in amplitude, $\mathrm{O}(10^{-5})$, and so evolved linearly. That means each Fourier mode evolved independently and hence can be described by a driven harmonic oscillator, with frequency determined by the sound speed in the fluid. Thus the fluid density oscillates, which gives oscillations in temperature, together with a velocity effect which is $\pi/2$ out of phase and has its amplitude reduced by the sound speed.

After the Universe recombined the baryons and radiation decoupled, and the radiation could travel freely towards us. At that point the phases of the oscillations were frozen-in, and projected on the sky as a harmonic series of peaks. The main peak is the mode that went through 1/4 of a period, reaching maximal compression. The even peaks are maximal *under*-densities, which are generally of smaller amplitude because the rebound has to fight against the baryon inertia. The troughs, which do not extend to zero power, are partially filled by the Doppler effect because they are at the velocity maxima.

An additional ingredient comes from geometrical projection. The scale associated with the peaks is the sound horizon at last scattering, which can be straightforwardly calculated as a physical length scale. This length is projected onto the sky, leading to an angular scale that depends on the background cosmology. Hence the angular position of the peaks is a sensitive probe of the spatial curvature of the Universe (*i.e.*, $\Omega_{\rm tot}$), with the peaks lying at higher ℓ in open universes and lower ℓ in closed geometry.

One last effect arises from reionization at redshift $z_{\rm i}$. A fraction of photons (τ) will be isotropically scattered at $z < z_{\rm i}$, partially erasing the anisotropies at angular scales smaller than those subtended by the Hubble radius at $z_{\rm i}$, which corresponds typically to ℓs above about a few 10s, depending on the specific reionization model. The acoustic peaks are therefore reduced by a factor $e^{-2\tau}$ relative to the plateau.

These peaks were a clear theoretical prediction going back to about 1970 [22]. One can think of them as a snapshot of stochastic standing waves. Since the physics governing them is simple and their structure rich, then one can see how they encode extractable information about the cosmological parameters. Their empirical existence started to become clear around 1994 [23], and the emergence, over the following decade, of a coherent series of acoustic peaks and troughs is a triumph of modern cosmology. This picture has received further confirmation with the recent detection in the power spectrum of galaxies (at redshifts close to zero) of the imprint of the acoustic oscillations in the baryon component [24].

23.4.3. *The damping tail:* $\ell \gtrsim 1000$:

The recombination process is not instantaneous, giving a thickness to the last scattering surface. This leads to a damping of the anisotropies at the highest ℓs, corresponding to scales smaller than that subtended by this thickness. One can also think of the photon-baryon fluid as having imperfect coupling, so that there is diffusion between the two components, and hence the amplitudes of the oscillations decrease with time. These effects lead to a damping of the C_ℓs, sometimes called Silk damping [25], which cuts off the anisotropies at multipoles above about 2000.

An extra effect at high ℓs comes from gravitational lensing, caused mainly by non-linear structures at low redshift. The C_ℓs are convolved with a smoothing function in a calculable way, partially flattening the peaks, generating a power-law tail at the highest multipoles, and complicating the polarization signal [26]. This is an example of a 'secondary effect', *i.e.*, the processing of anisotropies due to relatively nearby structures. Galaxies and clusters of galaxies give several such effects, but all are expected to be of low amplitude and are typically only important for the highest ℓs.

23.5. Current Anisotropy Data

There has been a steady improvement in the quality of CMB data that has led to the development of the present-day cosmological model. Probably the most robust constraints currently available come from the combination of the *WMAP* first year data [4] with smaller scale results from the CBI [27] and ACBAR [28] experiments. Newer data from BOOMERANG [29] and the VSA [30] are also useful at smaller angular scales and give consistent results for parameters. We plot power spectrum estimates from these five experiments in Fig. 23.2. Other recent experiments, such as ARCHEOPS [31], DASI [32] and MAXIMA [33] also give powerful constraints, which are quite consistent with what we describe below. There have been some comparisons among data-sets [34], which indicate very good agreement, both in maps and in derived power spectra (up to systematic uncertainties in the overall calibration for some experiments). This makes it clear that systematic effects are largely under control. However, a fully self-consistent joint analysis of all the current data sets has not been attempted, one of the reasons being that it requires a careful treatment of the overlapping sky coverage.

Fig. 23.2 shows band-powers from the first year *WMAP* data [35], together with BOOMERANG [29], VSA [30], CBI [27] and ACBAR [28] data at higher ℓ. The points are in very good agreement with a 'ΛCDM' type model, as described earlier, with several of the peaks and troughs quite apparent. For details of how these estimates were arrived at, the strength of any correlations between band-powers and other information required to properly interpret them, turn to the original papers.

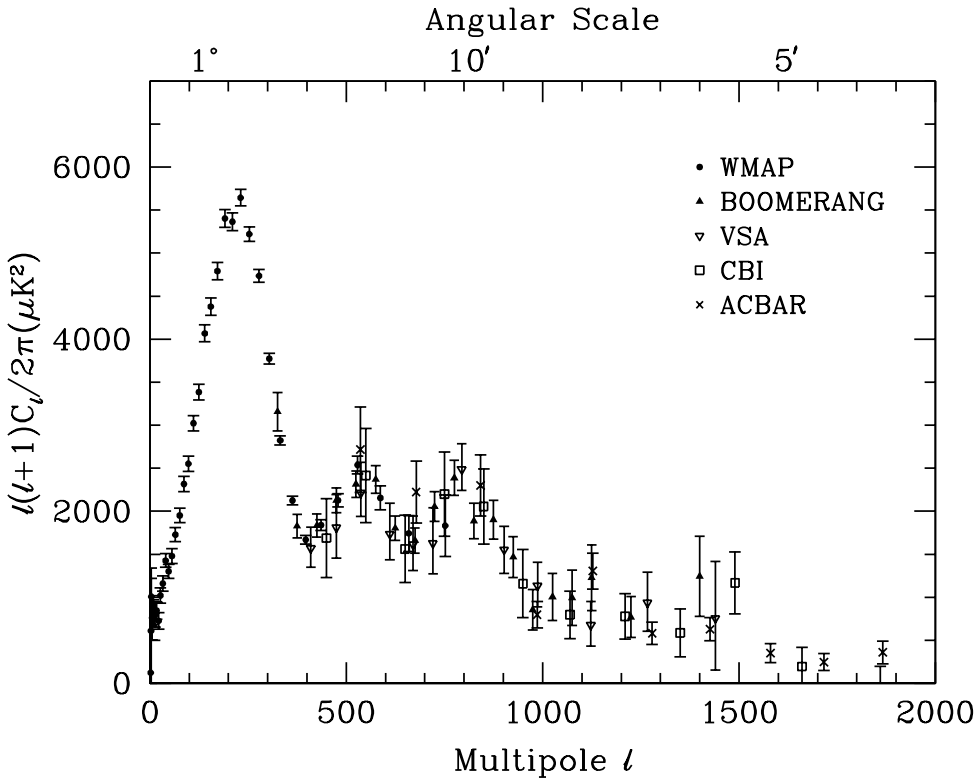

Figure 23.2: Band-power estimates from the *WMAP*, BOOMERANG, VSA, CBI, and ACBAR experiments. We have suppressed some of the low-ℓ and high-ℓ band-powers which have large error bars. Note also that the widths of the ℓ-bands varies between experiments. This plot represent only a selection of available experimental results, with some other data-sets being of similar quality. The multipole axis here is linear, so the Sachs-Wolfe plateau is hard to see. However, the acoustic peaks and damping region are very clearly observed, with no need for a theoretical curve to guide the eye.

23.6. CMB Polarization

Since Thomson scattering of an anisotropic radiation field also generates linear polarization, the CMB is predicted to be polarized at the roughly 5% level [36]. Polarization is a spin 2 field on the sky, and the algebra of the modes in ℓ-space is strongly analogous to spin-orbit coupling in quantum mechanics [37]. The linear polarization pattern can be decomposed in a number of ways, with two quantities required for each pixel in a map, often given as the Q and U Stokes parameters. However, the most intuitive and physical decomposition is a geometrical one, splitting the polarization pattern into a part that comes from a divergence (often referred to as the 'E-mode') and a part with a curl (called the 'B-mode') [38]. More explicitly, the modes are defined in terms of second derivatives of the polarization amplitude, with the Hessian for the E-modes having principle axes in the same sense as the polarization, while the B-mode pattern can be thought of simply as a 45° rotation of the E-mode pattern. Globally

one sees that the E-modes have $(-1)^\ell$ parity (like the spherical harmonics), while the B-modes have $(-1)^{\ell+1}$ parity.

The existence of this linear polarization allows for 6 different cross power spectra to be determined from data that measure the full temperature and polarization anisotropy information. Parity considerations make 2 of these zero, and we are left with 4 potential observables: $C_\ell^{\rm TT}$, $C_\ell^{\rm TE}$, $C_\ell^{\rm EE}$, and $C_\ell^{\rm BB}$. Since scalar perturbations have no handedness, the B-mode power spectrum can only be generated by vectors or tensors. Hence, in the context of inflationary models, the determination of a non-zero B-mode signal is a way to measure the gravity wave contribution (and thus potentially derive the energy scale of inflation), even if it is rather weak. However, one must first eliminate the foreground contributions and other systematic effects down to very low levels.

The oscillating photon-baryon fluid also results in a series of acoustic peaks in the polarization C_ℓs. The main 'EE' power spectrum has peaks that are out of phase with those in the 'TT' spectrum, because the polarization anisotropies are sourced by the fluid velocity. The 'TE' part of the polarization and temperature patterns comes from correlations between density and velocity perturbations on the last scattering surface, which can be both positive and negative, and is of larger amplitude than the EE signal. There is no polarization 'Sachs-Wolfe' effect, and hence no large-angle plateau. However, scattering during a recent period of reionization can create a polarization 'bump' at large angular scales.

The strongest upper limits on polarization are at the roughly $10\,\mu$K level from the POLAR [39] experiment at large angular scales and the PIQUE [40], COMPASS [41] and CBI [42] experiments at smaller scales. The first measurement of a polarization signal came in 2002 from the DASI experiment [43], which provided a convincing detection, confirming the general paradigm, but of low enough significance that it lent little constraint to models. As well as the E-mode signal, DASI also made a statistical detection of the TE correlation.

In 2003 the *WMAP* experiment demonstrated that is was able to measure the TE cross-correlation power spectrum with high precision [44]. Other recent experimental results include a weak detection of the EE signal from CAPMAP [45] and more significant detections from CBI [46], DASI [47] and BOOMERANG [48]. The TE signal has also been detected in several multipole bands by BOOMERANG [49], and there are statistical detections by CBI [46] and DASI [47]. Some upper limits on $C_\ell^{\rm BB}$ also exist, but are currently not very constraining.

The results of *WMAP* $C_\ell^{\rm TE}$ are shown in Fig. 23.3, along with estimates from the DASI and BOOMERANG experiments. The measured shape of the cross-correlation power spectrum provides supporting evidence of the adiabatic nature of the perturbations, as well as directly constraining the thickness of the last scattering surface. Since the polarization anisotropies are generated in this scattering surface, the existence of correlations at angles above about a degree demonstrate that there were super-Hubble fluctuations at the recombination epoch.

The most intriguing result from the polarization measurements is at the largest angular scales ($\ell < 10$), where there is an excess signal compared to that expected from the temperature power spectrum alone. This is precisely the signal expected from an early period of reionization, arising from Doppler shifts during the partial scattering at $z < z_{\rm i}$.

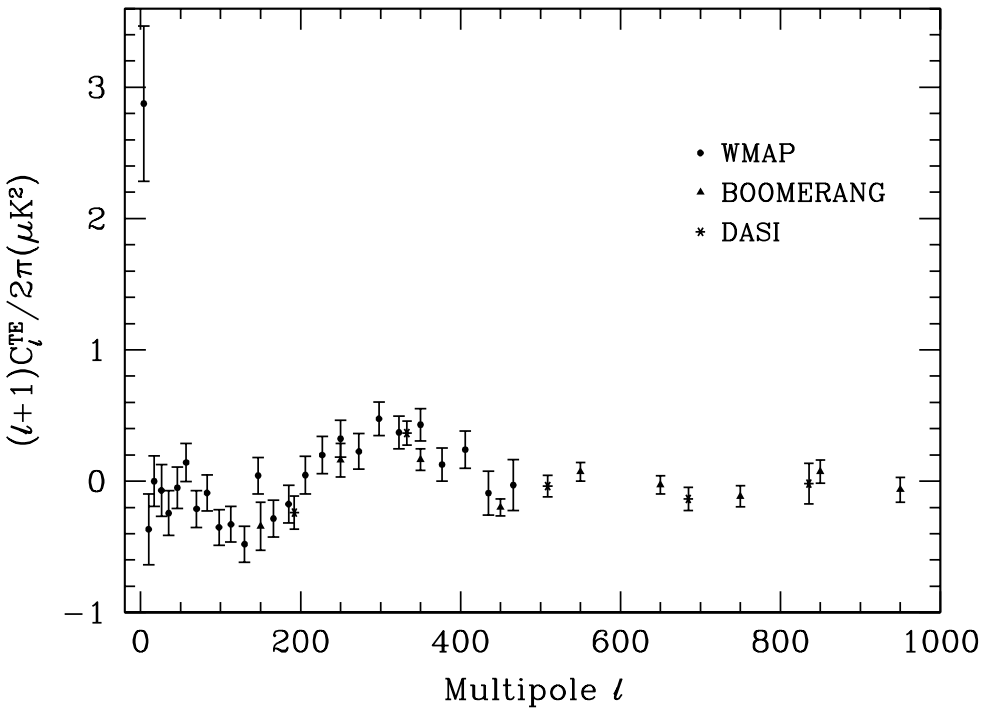

Figure 23.3: Cross power spectrum of the temperature anisotropies and E-mode polarization signal from *WMAP*, together with estimates from DASI and BOOMERANG which extend to higher ℓ. Note that the BOOMERANG bands are wider in ℓ than those of *WMAP*, while those of DASI are almost as wide as the features in the power spectrum. Also note that the y-axis here is not multiplied by the additional ℓ, which helps to show both the large and small angular scale features.

It seems to indicate that the first stars, presumably the source of the ionizing radiation, formed around $z = 20$ (although the uncertainty is still quite large).

23.7. Complications

There are a number of issues which complicate the interpretation of CMB anisotropy data, some of which we sketch out below.

23.7.1. *Foregrounds*:

The microwave sky contains significant emission from our Galaxy and from extra-galactic sources [50]. Fortunately, the frequency dependence of these various sources is in general substantially different from that of the CMB anisotropy signals. The combination of Galactic synchrotron, bremsstrahlung and dust emission reaches a minimum at a wavelength of roughly 3 mm (or about 100 GHz). As one moves to greater angular resolution, the minimum moves to slightly higher frequencies, but becomes more sensitive to unresolved (point-like) sources.

At frequencies around 100 GHz and for portions of the sky away from the Galactic Plane the foregrounds are typically 1 to 10% of the CMB anisotropies. By making

observations at multiple frequencies, it is relatively straightforward to separate the various components and determine the CMB signal to the few per cent level. For greater sensitivity it is necessary to improve the separation techniques by adding spatial information and statistical properties of the foregrounds compared to the CMB.

The foregrounds for CMB polarization are expected to follow a similar pattern, but are less well studied, and are intrinsically more complicated. Whether it is possible to achieve sufficient separation to detect B-mode CMB polarization is still an open question. However, for the time being, foreground contamination is not a major issue for CMB experiments.

23.7.2. *Secondary Anisotropies*:

With increasingly precise measurements of the primary anisotropies, there is growing theoretical and experimental interest in 'secondary anisotropies.' Effects which happen at $z \ll 1000$ become more important as experiments push to higher angular resolution and sensitivity.

These secondary effects include gravitational lensing, patchy reionization and the Sunyaev-Zel'dovich (SZ) effect [51]. This is Compton scattering ($\gamma e \to \gamma' e'$) of the CMB photons by a hot electron gas, which creates spectral distortions by transferring energy from the electrons to the photons. The effect is particularly important for clusters of galaxies, through which one observes a partially Comptonized spectrum, resulting in a decrement at radio wavelengths and an increment in the submillimeter. This can be used to find and study individual clusters and to obtain estimates of the Hubble constant. There is also the potential to constrain the equation of state of the Dark Energy through counts of detected clusters as a function of redshift [52].

23.7.3. *Higher-order Statistics*:

Although most of the CMB anisotropy information is contained in the power spectra, there will also be weak signals present in higher-order statistics. These statistics can measure any primordial non-Gaussianity in the perturbations, as well as non-linear growth of the fluctuations on small scales and other secondary effects (plus residual foreground contamination). Although there are an infinite variety of ways in which the CMB could be non-Gaussian, there is a generic form to consider for the initial conditions, where a quadratic contribution to the curvature perturbations is parameterized through a dimensionless number $f_{\rm NL}$. This weakly non-linear component can be constrained through measurements of the bispectrum or Minkowski functionals for example, and the result from *WMAP* is $-58 < f_{\rm NL} < 134$ (95% confidence region) [10].

23.8. Constraints on Cosmologies

The clearest outcome of the newer experimental results is that the standard cosmological paradigm is in good shape. A large amount of high precision data on the power spectrum is adequately fit with fewer than 10 free parameters. The framework is that of Friedmann-Robertson-Walker models, which have nearly flat geometry, containing Dark Matter and Dark Energy, and with adiabatic perturbations having close to scale invariant initial conditions.

Within this framework, bounds can be placed on the values of the cosmological parameters. Of course, much more stringent constraints can be placed on models which

cover a restricted number of parameters, e.g. assuming that $\Omega_{\rm tot} = 1$, $n = 1$ or $r = 0$. More generally, the constraints depend upon the adopted priors, even if they are implicit, for example by restricting the parameter freedom or the ranges of parameters (particularly where likelihoods peak near the boundaries), or by using different choices of other data in combination with the CMB. When the data become even more precise, these considerations will be less important, but for now we caution that restrictions on model space and choice of priors need to be kept in mind when adopting specific parameter values and uncertainties.

There are some combinations of parameters that fit the CMB anisotropies almost equivalently. For example, there is a nearly exact geometric degeneracy, where any combination of $\Omega_{\rm M}$ and Ω_Λ that gives the same angular diameter distance to last scattering will give nearly identical C_ℓs. There are also other near degeneracies among the parameters. Such degeneracies can be broken when using the CMB data in combination with other cosmological data sets. Particularly useful are complementary constraints from galaxy clustering, the abundance of galaxy clusters, weak gravitational lensing measurements, Type Ia supernova distances and the distribution of Lyman α forest clouds. For an overview of some of these other cosmological constraints, see The Cosmological Parameters—Sec. 21 of this *Review*.

The combination of *WMAP*, CBI and ACBAR, together with weak priors (on h and $\Omega_{\rm B}h^2$ for example), and within the context of a 6 parameter family of models (which fixes $\Omega_{\rm tot} = 1$ and $r = 0$), yields the following results [53]: $A = 2.7(\pm 0.3) \times 10^{-9}$, $n = 0.97 \pm 0.03$, $h = 0.73 \pm 0.05$, $\Omega_{\rm B}h^2 = 0.023 \pm 0.001$, $\Omega_{\rm M}h^2 = 0.13 \pm 0.01$ and $\tau = 0.17 \pm 0.07$. Other combinations of data, e.g. including BOOMERANG and other newer CMB measurements, or improved large-scale structure data, lead to consistent results, sometimes with smaller error bars, and with the precise values depending on data selection [54]. Note that for h, the CMB data alone provide only a very weak constraint, unless spatial flatness or some other cosmological data are used. For $\Omega_{\rm B}h^2$ the precise value depends sensitively on how much freedom is allowed in the shape of the primordial power spectrum (see Big-Bang nucleosynthesis—Sec. 20 of this *Review*).

The best constraint on $\Omega_{\rm tot}$ is 1.02 ± 0.02. This comes from including priors from h and supernova data. However, slightly different, but consistent results come from using other data combinations.

The 95% confidence upper limit on r is 0.53 (including some extra constraint from galaxy clustering). This limit is stronger if we restrict ourselves to $n < 1$ and weaker if we allow $dn/d\ln k \neq 0$.

There are also constraints on parameters over and above the basic 8 that we have described. But for such constraints it is necessary to include additional data in order to break the degeneracies. For example the addition of the Dark Energy equation of state, w adds the partial degeneracy of being able to fit a ridge in (w, h) space, extending to low values of both parameters. This degeneracy is broken when the CMB is used in combination with independent H_0 limits, for example [13], giving $w < -0.5$ at 95% confidence. Tighter limits can be placed using restricted model-spaces and/or additional data.

For the optical depth τ, the error bar is large enough that apparently quite different results can come from other combinations of data. The constraint from the combined

WMAP $C_\ell^{\rm TT}$ and $C_\ell^{\rm TE}$ data is $\tau = 0.17 \pm 0.04$, which corresponds (within reasonable models) to a reionization redshift $9 < z_{\rm i} < 30$ (95% CL) [44]. This is a little higher than some theoretical predictions and some indications from studies of absorption in high-z quasar spectra [56]. The excitement here is that we have direct information from CMB polarization which can be combined with other astrophysical measurements to understand when the first stars formed and brought about the end of the cosmic dark ages.

23.9. Particle Physics Constraints

CMB data are beginning to put limits on parameters which are directly relevant for particle physics models. For example there is a limit on the neutrino contribution $\Omega_\nu h^2 < 0.0076$ (95% confidence) from a combination of *WMAP* and galaxy clustering data from the 2dFGRS project [57]. This directly implies a limit on neutrino mass, $\sum m_\nu < 0.7\,{\rm eV}$, assuming the usual number density of fermions which decoupled when they were relativistic.

A combination of the *WMAP* data with other data-sets gives some hint of a running spectral index, *i.e.*, $dn/d\ln k \neq 0$ [53]. Although this is still far from resolved [58], things will certainly improve as new data come in. A convincing measurement of a non-zero running of the index would be quite constraining for inflationary models [59].

One other hint of new physics lies in the fact that the quadrupole and some of the other low ℓ modes seem anomalously low compared with the best-fit ΛCDM model [35]. This is what might be expected in a universe which has a large scale cut-off to the power spectrum, or is topologically non-trivial. However, because of cosmic variance, possible foregrounds, apparent correlations between modes (as mentioned in Sec. 23.2), *etc.*, the significance of this feature is still a matter of debate [12,60].

In addition it is also possible to put limits on other pieces of physics [61], for example the neutrino chemical potentials, contribution of warm dark matter, decaying particles, time variation of the fine-structure constant, or physics beyond general relativity. Further particle physics constraints will follow as the anisotropy measurements increase in precision.

Careful measurement of the CMB power spectra and non-Gaussianity can in principle put constraints on physics at the highest energies, including ideas of string theory, extra dimensions, colliding branes, *etc.* At the moment any calculation of predictions appears to be far from definitive. However, there is a great deal of activity on implications of string theory for the early Universe, and hence a very real chance that there might be observational implications for specific scenarios.

23.10. Fundamental Lessons

More important than the precise values of parameters is what we have learned about the general features which describe our observable Universe. Beyond the basic hot Big Bang picture, the CMB has taught us that:

- The Universe recombined at $z \simeq 1100$ and started to become ionized again at $z \simeq 10$–30.
- The geometry of the Universe is close to flat.
- Both Dark Matter and Dark Energy are required.

- Gravitational instability is sufficient to grow all of the observed large structures in the Universe.
- Topological defects were not important for structure formation.
- There are 'synchronized' super-Hubble modes generated in the early Universe.
- The initial perturbations were adiabatic in nature.
- The perturbations had close to Gaussian (*i.e.*, maximally random) initial conditions.

It is very tempting to make an analogy between the status of the cosmological 'Standard Model' and that of particle physics. In cosmology there are about 10 free parameters, each of which is becoming well determined, and with a great deal of consistency between different measurements. However, none of these parameters can be calculated from a fundamental theory, and so hints of the bigger picture, 'physics beyond the Standard Model' are being searched for with ever more ambitious experiments.

Despite this analogy, there are some basic differences. For one thing, many of the cosmological parameters change with cosmic epoch, and so the measured values are simply the ones determined today, and hence they are not 'constants', like particle masses for example (although they *are* deterministic, so that if one knows their values at one epoch, they can be calculated at another). Moreover, the number of parameters is not as fixed as it is in the particle physics Standard Model; different researchers will not necessarily agree on what the free parameters are, and new ones can be added as the quality of the data improves. In addition, parameters like τ, which come from astrophysics, are in principle calculable from known physical processes, although this is currently impractical. On top of all this, other parameters might be 'stochastic' in that they may be fixed only in our observable patch of the Universe or among certain vacuum states in the 'Landscape' [62].

In a more general sense the cosmological 'Standard Model' is much further from the underlying 'fundamental theory' which will ultimately provide the values of the parameters from first principles. Nevertheless, any genuinely complete 'theory of everything' must include an explanation for the values of these cosmological parameters as well as the parameters of the Standard Model of particle physics.

23.11. Future Directions

With all the observational progress in the CMB and the tying down of cosmological parameters, what can we anticipate for the future? Of course there will be a steady improvement in the precision and confidence with which we can determine the appropriate cosmological model and its parameters. We can anticipate that the evolution from one year to four years of *WMAP* data will bring improvements from the increased statistical accuracy and from the more detailed treatment of calibration and systematic effects. Ground-based experiments operating at smaller angular scales will also improve over the next few years, providing significantly tighter constraints on the damping tail. In addition, the next CMB satellite mission, *Planck*, is scheduled for launch in 2007, and there are even more ambitious projects currently being discussed.

Despite the increasing improvement in the results, it is also true that the addition of the latest experiments has not significantly changed the cosmological model (apart from a suggestion of higher reionization redshift perhaps). It is therefore appropriate to ask: what should we expect to come from *Planck* and from other more grandiose future

experiments, including those being discussed as part of the 'Beyond Einstein' initiative? *Planck* certainly has the advantage of high sensitivity and a full sky survey. A detailed measurement of the third acoustic peak provides a good determination of the matter density; this can only be done by measurements which are accurate relative to the first two peaks (which themselves constrain the curvature and the baryon density). A detailed measurement of the damping tail region will also significantly improve the determination of n and any running of the slope. *Planck* should also be capable of measuring $C_\ell^{\rm EE}$ quite well, providing both a strong check on the cosmological Standard Model and extra constraints that will improve parameter estimation.

A set of cosmological parameters are now known to roughly 10% accuracy, and that may seem sufficient for many people. However, we should certainly demand more of measurements which describe *the entire observable Universe*! Hence a lot of activity in the coming years will continue to focus on determining those parameters with increasing precision. This necessarily includes testing for consistency among different predictions of the cosmological Standard Model, and searching for signals which might require additional physics.

A second area of focus will be the smaller scale anisotropies and 'secondary effects.' There is a great deal of information about structure formation at $z \ll 1000$ encoded in the CMB sky. This may involve higher-order statistics as well as spectral signatures. Such investigations can also provide constraints on the Dark Energy equation of state, for example. *Planck*, as well as experiments aimed at the highest ℓs, should be able to make a lot of progress in this arena.

A third direction is increasingly sensitive searches for specific signatures of physics at the highest energies. The most promising of these may be the primordial gravitational wave signals in $C_\ell^{\rm BB}$, which could be a probe of the $\sim 10^{16}$ GeV energy range. Whether the amplitude of the effect coming from inflation will be detectable is unclear, but the prize makes the effort worthwhile.

Anisotropies in the CMB have proven to be the premier probe of cosmology and the early Universe. Theoretically the CMB involves well-understood physics in the linear regime, and is under very good calculational control. A substantial and improving set of observational data now exists. Systematics appear to be well understood and not a limiting factor. And so for the next few years we can expect an increasing amount of cosmological information to be gleaned from CMB anisotropies, with the prospect also of some genuine surprises.

References:

1. A.A. Penzias and R. Wilson, Astrophys. J. **142**, 419 (1965);
   R.H. Dicke *et al.*, Astrophys. J. **142**, 414 (1965).
2. M. White, D. Scott, and J. Silk, Ann. Rev. Astron. & Astrophys. **32**, 329 (1994);
   W. Hu and S. Dodelson, Ann. Rev. Astron. & Astrophys. **40**, 171 (2002).
3. G.F. Smoot *et al.*, Astrophys. J. **396**, L1 (1992).
4. C.L. Bennett *et al.*, Astrophys. J. Supp. **148**, 1 (2003).
5. J.C. Mather *et al.*, Astrophys. J. **512**, 511 (1999).

6. S. Courteau *et al.*, Astrophys. J. **544**, 636 (2000).
7. D.J. Fixsen *et al.*, Astrophys. J. **420**, 445 (1994).
8. D.J. Fixsen *et al.*, Astrophys. J. **473**, 576 (1996);
   A. Kogut *et al.*, Astrophys. J. **419**, 1 (1993).
9. S. Seager, D.D. Sasselov, and D. Scott, Astrophys. J. Supp. **128**, 407 (2000).
10. E. Komatsu *et al.*, Astrophys. J. Supp. **148**, 119 (2003).
11. N. Bartolo *et al.*, Phys. Rep. **402**, 103 (2004).
12. A. de Oliveira-Costa *et al.*, Phys. Rev. **D69**, 063516 (2004).
13. Eriksen H.K. *et al.*, Astrophys. J. **605**, 14 (2004);
    P. Vielva *et al.*, Astrophys. J. **609**, 22 (2004);
    D.L. Larson, B.D. Wandelt, Astrophys. J. **613**, L85 (2004);
    P. Bielewicz, K.M. Gorski, and A.J. Banday, Monthly Not. Royal Astron. Soc. **355**, 1283 (2004);
    S. Prunet *et al.*, Phys. Rev. **D71**, 083508 (2005);
    Eriksen H.K. *et al.*, Astrophys. J. **622**, 58 (2005).
14. L. Knox, Phys. Rev. **D52**, 4307 (1995).
15. A.R. Liddle and D.H. Lyth, Cosmological Inflation and Large-Scale Structure, Cambridge University Press (2000).
16. U. Seljak and M. Zaldarriaga, Astrophys. J. **469**, 437 (1996).
17. A. Lewis, A. Challinor, A. Lasenby, Astrophys. J. **538**, 473 (2000).
18. U. Seljak *et al.*, Phys. Rev. **D68**, 083507 (2003).
19. R.K. Sachs and A.M. Wolfe, Astrophys. J. **147**, 73 (1967).
20. M.R. Nolta *et al.*, Astrophys. J. **608**, 10 (2004);
    S. Boughn and R. Crittenden, Nature, **427**, 45 (2004);
    P. Fosalba, E. Gaztañaga, and F. Castander, Astrophys. J. **597**, L89 (2003);
    N. Afshordi, Y.-S. Loh, and M.A. Strauss, Phys. Rev. **D69**, 083524 (2004);
    N. Padmanabhan *et al.*, Phys. Rev. D in press `astro-ph/0410360`.
21. W. Hu and D.J. Eisenstein, Phys. Rev. **D59**, 083509 (1999);
    W. Hu *et al.*, Phys. Rev. **D59**, 023512 (1999).
22. P.J.E. Peebles and J.T. Yu, Astrophys. J. **162**, 815 (1970);
    R.A. Sunyaev and Ya.B. Zel'dovich, Astrophysics & Space Science **7**, 3 (1970).
23. D. Scott, J. Silk, and M. White, Science **268**, 829 (1995).
24. D.J. Eisenstein *et al.*, Astrophys. J. in press `astro-ph/0501171`;
    S. Cole *et al.*, Monthly Not. Royal Astron. Soc. in press, `astro-ph/0501174`.
25. J. Silk, Astrophys. J. **151**, 459 (1968).
26. M. Zaldarriaga and U. Seljak, Phys. Rev. **D58**, 023003 (1998).
27. T.J. Pearson *et al.*, Astrophys. J. **591**, 556 (2003);

A.C.S. Readhead *et al.*, Astrophys. J. **609**, 498 (2004).

28. M.C. Runyan *et al.*, Astrophys. J. Supp. **149**, 265 (2003);
C.L. Kuo *et al.*, Astrophys. J. **600**, 32 (2004).
29. J.E. Ruhl *et al.*, Astrophys. J. **599**, 786 (2003);
S. Masi *et al.*, Astrophys. J. in press `astro-ph/0507509`;
W.C. Jones *et al.*, Astrophys. J. in press `astro-ph/0507494`.
30. P.F. Scott *et al.*, Monthly Not. Royal Astron. Soc. **341**, 1076 (2003);
Grainge K. *et al.*, Monthly Not. Royal Astron. Soc. **341**, L23 (2003);
C. Dickinson *et al.*, Monthly Not. Royal Astron. Soc. **353**, 732 (2004).
31. A. Benoit *et al.*, Astronomy & Astrophysics **399**, L19 (2003);
M. Tristram *et al.*, Astronomy & Astrophysics **436**, 785 (2003).
32. N.W. Halverson *et al.*, Astrophys. J. **568**, 38 (2002).
33. A.T. Lee *et al.*, Astrophys. J. **561**, L1 (2001).
34. M.E. Abroe *et al.*, Astrophys. J. **605**, 607 (2004);
N. Rajguru *et al.*, Astrophys. J. in press `astro-ph/0502330`.
35. G. Hinshaw *et al.*, Astrophys. J. Supp. **148**, 135 (2003).
36. W. Hu, M. White, New Astron. **2**, 323 (1997).
37. W. Hu, M. White, Phys. Rev. **D56**, 596 (1997).
38. M. Zaldarriaga and U. Seljak, Phys. Rev. **D55**, 1830 (1997);
M. Kamionkowski, A. Kosowsky, and A. Stebbins, Phys. Rev. **D55**, 7368 (1997).
39. B.G. Keating *et al.*, Astrophys. J. **560**, L1 (2001).
40. M.M. Hedman *et al.*, Astrophys. J. **548**, L111 (2001).
41. P.C. Farese *et al.*, Astrophys. J. **610**, 625 (2004).
42. J.K. Cartwright *et al.*, Astrophys. J. **623**, 11 (2005).
43. J. Kovac *et al.*, Nature, 420, 772 (2002).
44. A. Kogut *et al.*, Astrophys. J. Supp. **148**, 161 (2003).
45. D. Barkats *et al.*, Astrophys. J. **619**, L127 (2005).
46. A.C.S. Readhead *et al.*, Science, **306**, 836 (2004).
47. E.M. Leitch *et al.*, Astrophys. J. **624**, 10 (2005).
48. T.E. Montroy *et al.*, Astrophys. J. in press `astro-ph/0507514`.
49. F. Piacentini *et al.*Astrophys. J. in press `astro-ph/0507507`.
50. A. de Oliveira-Costa, M. Tegmark (eds.), Microwave Foregrounds, Astron. Soc. of the Pacific, San Francisco (1999).
51. R.A. Sunyaev and Ya.B. Zel'dovich, Ann. Rev. Astron. Astrophys. **18**, 537 (1980);
M. Birkinshaw, Phys. Rep. **310**, 98 (1999).
52. J.E. Carlstrom, G.P. Holder, and E.D. Reese, Ann. Rev. Astron. & Astrophys. **40**, 643 (2002).

53. D.N. Spergel *et al.*, Astrophys. J. Supp. **148**, 175 (2003).
54. M. Tegmark *et al.*, Phys. Rev. **D69**, 103501 (2004);
C.J. MacTavish *et al.*, Astrophys. J. in press `astro-ph/0507503`;
A.G. Sánchez *et al.*, Monthly Not. Royal Astron. Soc. in press, `astro-ph/0507583`.
55. W.L. Freedman *et al.*, Astrophys. J. **553**, 47 (2001).
56. X. Fan *et al.*, Astrophys. J. **123**, 1247 (2002).
57. M. Colless *et al.*, Monthly Not. Royal Astron. Soc. **328**, 1039 (2001).
58. U. Seljak, P. McDonald, and A. Makarov, Monthly Not. Royal Astron. Soc. **342**, L79 (2003).
59. H.V. Peiris *et al.*, Astrophys. J. Supp. **148**, 213 (2003).
60. G. Efstathiou, Monthly Notices of the Royal Astronomical Society, **346**, L26 (2003).
61. M. Kamionkowski and A. Kosowsky, Ann. Rev. Nucl. Part. Sci. **49**, 77 (1999).
62. L. Susskind, The Davis Meeting On Cosmic Inflation (2003), `hep-th/0302219`.